07,01

Dynamic hardness and formation of Portevin–Le Chatelier bands during impact indentation

© A.A. Shibkov, A.E. Zolotov, A.A. Denisov, M.F. Gasanov, E.A. Shibkov, S.S. Kochegarov

Tambov State University,
Tambov, Russia

E-mail: shibkovaleks@mail.ru

Received February 22, 2023
Revised February 22, 2023
Accepted March 1, 2023

The effect of shock indentation on the formation and propagation of the Portevin–Le Chatelier deformation bands in an aluminum-magnesium alloy was studied experimentally using acoustic emission and high-speed video recording methods. Dynamic and nonlinear responses to shock indentation are revealed: the first include high values of dynamic hardness and local strain and loading rates, and the second - threshold and multiple nature of force and acoustic responses. It is shown that the bands of macrolocalized deformation represent a latent bulk type of erosion damage, which reduces the mechanical stability and durability of the alloy.

Keywords: contact shock, Portevin–Le Chatelier effect, deformation bands, fracture, aluminum-magnesium alloy.

DOI: 10.21883/PSS.2023.04.55998.23

1. Introduction

The most well-known manifestation of the collective dislocation dynamics at macrolevel is discontinuous deformation of metals and alloys or the Portevin–Le Chatelier effect (PLC) that consists in spontaneous formation of macrolocalized deformation bands in a plastically deformed material, which is accompanied by irregularities emerging on stress-strain curves [1]. Depending on conditions of the deformation process, these irregularities can be in the form of repeated stress drops or deformation jumps. If a force law $\sigma = \sigma(t)$ of the impact on the material is defined, usually $\dot{\sigma}_0 = \text{const}$ and response to the development of plastic instabilities has a form of repeated deformation drops $\Delta\varepsilon$ on $\varepsilon(\sigma)$ curves; if a deformation rate $\dot{\varepsilon} = \dot{\varepsilon}(t)$ is defined, then, as a rule $\dot{\varepsilon}_0 = \text{const}$ and response has a form of stress drops $\Delta\sigma$ on $\sigma(\varepsilon)$ stress-strain curves. The first situation corresponds to the direct problem of nonlinear dynamics when forces are given and the response is unsteady elastic-plastic deformation, and the second situation corresponds to the inverse problem when the flux $\dot{\varepsilon}_0$ is given and the force response is investigated. It is the situation, the most of PLC effect studies are focused on. At the same time, the less studied first situation corresponds to a greater extent to the conditions of operation and processing of metal alloys, when forces are defined (traction force, lifting force, drag force, friction force, pressure of forming, etc.) and the response is the unsteady deformation of material or structure.

Despite the more than hundred-years history of discontinuous deformation studies [1–3] and half-century investigations of deformation bands [4–9], the nature of these phenomena is still unclear and is a subject of continuing discussion about mechanisms of the spontaneous nucleation and propagation of localized deformation bands causing jumps on tensile (compression) diagrams. In practice, the bands have a negative effect on strength, durability and corrosion resistance of metals and alloys. In addition, the industrial alloys that demonstrate the PLC effect are exposed to external process impacts in the course of metal processing and operation (laser processing or shot blasting, exposure to corrosion chemical media, etc.), which may provoke the nucleation of deformation bands near the loaded members of structure assemblies. To forecast behavior of such alloys under external high-energy impacts, it is necessary to investigate mechanisms of their effect on the formation of deformation bands, which dynamics finally results in destruction of the material. The purpose of this study is to investigate the effect of contact impact on nucleation and propagation of bands in a deformed alloy that demonstrate the PLC effect, which is chosen to be AMg6, an aluminum-magnesium alloy that is widely used in manufacturing of aviation and automotive vehicles.

2. Technique

Samples of the AMg6 industrial aluminum-magnesium alloy (Al — 6.15%, Mg — 0.65%, Mn — 0.25%, Si — 0.21% Fe; wt%) in the form of hourglass with a working part size of $6 \times 3 \times 0.5$ mm were cut from cold-rolled sheet along the direction of rolling. Two types of samples were investigated: AMg6-I with recrystallized structure resulted from a 2-hr annealing at 450°C and air quenching and samples of AMg6-II work-hardened by cold rolling to a true strain of $e \approx 3$. Structure of samples after heat treatment and machining is described in [10]. Fig. 1 shows typical tensile curves of AMg6-I and AMg6-II samples at a constant rate of growth of the applied stress ($\dot{\sigma}_0 = 0.2$ MPa/s). AMg6-I samples demonstrate stepwise loading curves and

Mechanical properties of AMg6 alloy samples

Types of samples	H_V, MPa	σ_B MPa	$\sigma_{0.2}$, MPa	δ, %	ε_c, %	ρ_0, cm^{-2} [10]	N_j	$\Delta\varepsilon$, %
AMg6-I	800	330	160	35	2	10^8	8–10	1–10
AMg6-II	1200	400	330	16	9	10^{12}	1	2–3

Note. H_V is Vickers microhardness, σ_B is ultimate strength, $\sigma_{0.2}$ is offset yield strength, δ is relative deformation before destruction, ε_c is deformation of the first jump, ρ_0 is initial density of dislocations, N_j is number of deformation jumps on tensile curves, $\Delta\varepsilon$ is amplitude of deformation jumps.

AMg6-II samples have smooth curves without jumps, except for the deformation jump with the necking and sample destruction. The table presents main mechanical properties of these samples.

In the process of tensile loading the samples were subjected to dynamic (shock) indentation at different levels of applied stress. The shock of indenter under certain conditions provoked development of an induced (premature) deformation jump on the tensile curve, nucleation of macrolocalized deformation bands in the indentation zone and their propagation. To study the dynamics of bands, the acoustic emission (AE) methods was used in combination with high-speed video recording with a rate of up to 20 000 frames per second (fps) by a FASTCAM Mini UX50/100 Photron high-speed digital camera. The acoustic signal turns on a Zetlab BC 601 acoustic emission transducer a AEP5 preamplifier (Vallen-Systeme) that records the AE signal in the frequency band from ~ 30 to ~ 600 kHz. A Vickers pyramid was used as indenter.

The schematic diagram of experimental setup shown in Fig. 2 includes a sample *1* stretched at a constant rate of stress growth $\dot{\sigma}_0 = \text{const}$, an acoustic sensor *2* attached to the lower blade of the sample, a Vickers indenter *3* driven by explosion of a compact explosive charge *4* installed in a steel cylinder *5*. The indenter was suspended on a light bronze tape *6*. Explosion of the explosive charge was initiated by a pulse of the *7* (YLP-1-100-50-50-HC-RG infrared fiber laser with a radiation wavelength of 1064 nm, a nominal pulse energy of 1 mJ, a pulse repetition frequency of 50 kHz, a pulse length of 120 ns) with a radiation flux density at the

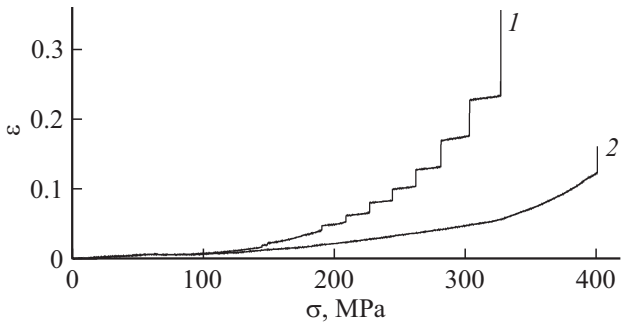

Figure 1. Curves of loading at a rate of $\dot{\sigma}_0 = 0.2$ MPa/s for samples of AMg6-I (*1*) and AMg6-II (*2*) alloys.

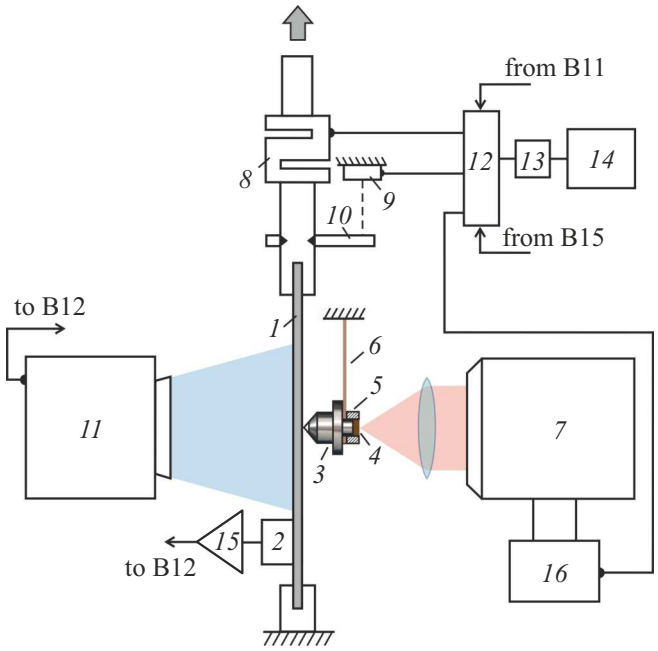

Figure 2. Schematic diagram of the experimental setup. *1* — sample, *2* — piezoelectric transducer, *3* — indenter, *4* — explosive charge, *5* — steel cylinder, *6* — light suspension, *7* — pulse IR-laser, *8* — strain gauge, *9* — laser position sensor, *10* — mirror, *11* — high-speed camera, *12* — switch, *13* — ADC, *14* — computer, *15* — preamplifier of AE signal, *16* — external laser control unit.

ficus of $\sim 10^6$ W/cm^2. The force response was recorded by a strain gauge *8* (Zemic H3-C3-100 kg-3B with a sensitivity of 1.5 V/N), the sample deformation was measured by a laser triangulating sensor of position *9* (Riftec, with a sensitivity of 1.5 μm in the frequency band of up to 2 kHz), which recorded the distance between the base and the mirror *10* attached on a movable stem of the test machine. The surface of flat sample opposite to the shock impact was video-recorded by a high-speed camera *11*. To synchronize recorded signals of the AE sensor, the force transducer, the position sensor, the laser control unit and the video camera, these signals were supplied to a switch *12* followed by an analog-to-digital converter (ADC) *13* and a computer *14*. To initiate the explosion of an explosive granule by laser radiation, the „free running“ laser mode for 1 ms was used. Time of the laser generation was set by a rectangular pulse of voltage with a length of 1 ms in the mode of external control of the laser by the control unit *16*. The Vickers microhardness was measured by PMT-3 microhardness tester at a load of 20 g for 10 s.

3. Experimental results

Samples of AMg6-I alloy demonstrate an explicit stepwise tensile curve (Fig. 1, curve *1*). An increase in the applied stress results in growth of the jump amplitude $\Delta\varepsilon$ and the

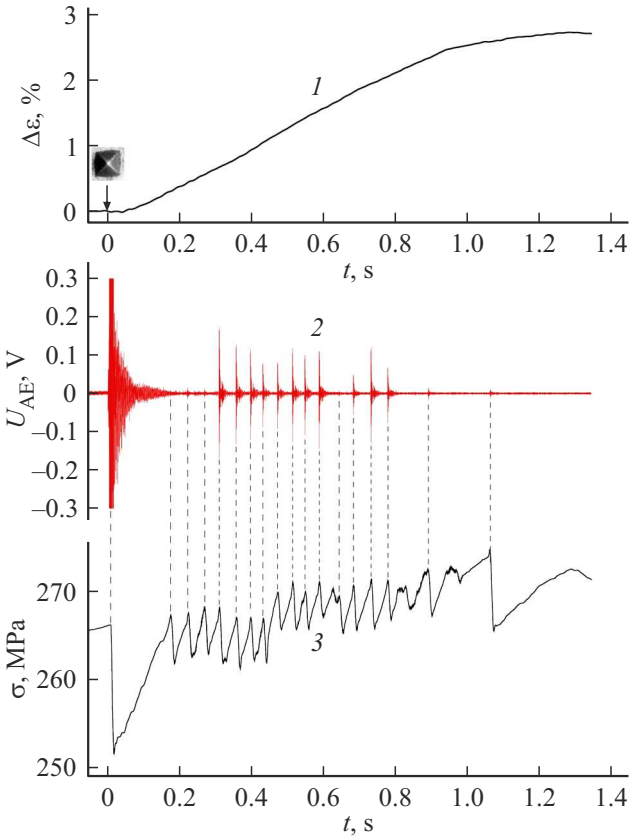

Figure 3. Synchronous records of signals from transducers of deformation (*1*), acoustic emission (*2*) and force (*3*) under a shock indentation of the AMg6 alloy sample surface being deformed. The arrow shows the moment of shock. The insert shows the indent after the shock.

plateau $\Delta\sigma$ between the jumps [11] and, respectively, the length of plateau $\Delta t = \Delta\sigma/\sigma_0$, so that

$$\Delta\sigma = a\Delta\varepsilon^n, \qquad (1)$$

where a and n are constants that depend on the alloy grade. Dependence (1) is typical for aluminum-magnesium alloys with the Mg percentage from 2 to 6%. For the AMg6-I alloy: $a = 45$ MPa, $n = 0.273$ at $T = 300$ K. In [11,12] it has been found empirically that the last third of the plateau is the most sensitive to external impacts, in particular, to the effect of corrosion medium [12] and to the pulse laser IR-emission [11]. It is found that the shock indentation of surface of the AMg6-I alloy sample being deformed demonstrate a qualitatively similar behavior: the first third of the plateau in fact is insensitive to the shock impact and in the last third of the plateau the amplitude of induced deformation jump achieves 60–80% of the amplitude of spontaneous jump and in the middle third of the plateau the relative amplitude increases respectively from zero to almost 60% with increase in the applied stress.

To quantitatively investigate the deformation response to shock indentation, a plateau between high-amplitude jumps was chosen, for example, between the 5-th and the 6-th jumps (Fig. 1) with a duration of $\Delta t = t_6 - t_5 \approx 50$ s. The sample to be deformed within this plateau was subjected to a shock indentation to the center of the working part of sample with an interval of $\Delta\tau \approx 30$ s in relation to the start of the plateau, the shape and amplitude of the induced jump $\Delta\varepsilon_i$, the force and acoustic responses were measured and the dynamics and morphology of the deformation bands resulted from the indenter shock and subsequent development of the deformation jump were investigated.

Fig. 3 shows synchronous records of signals from transducers of deformation *1*, acoustic emission *2* and force *3* caused by the Vickers indenter shock. As can be seen from the figure, the indenter shock causes a „premature" development of deformation jump with an amplitude of about 3% (curve *1* in Fig. 3), typical repeated bursts of AE signals (curve *2*) and stress jumps in the force response (curve *3*). Amplitude of the first AE bursts caused by the indenter shock is significantly higher than amplitudes of subsequent AE signals. The results of video recording at a rate of 2000 fps show that AE burst in the deformation jump front are related to the formation of deformation bands and each AE burst has its corresponding process of single band formation (signal amplitude falls on the initial phase of development of a complete band) and a jump of machine–sample system unloading (Fig. 4).

Thus, a single indenter shock causes multiple force and acoustic responses within about one second after the shock impact, which are accompanied by formation and propagation of about ten deformation bands. The nonlinear behavior of the deformed material after a contact shock is

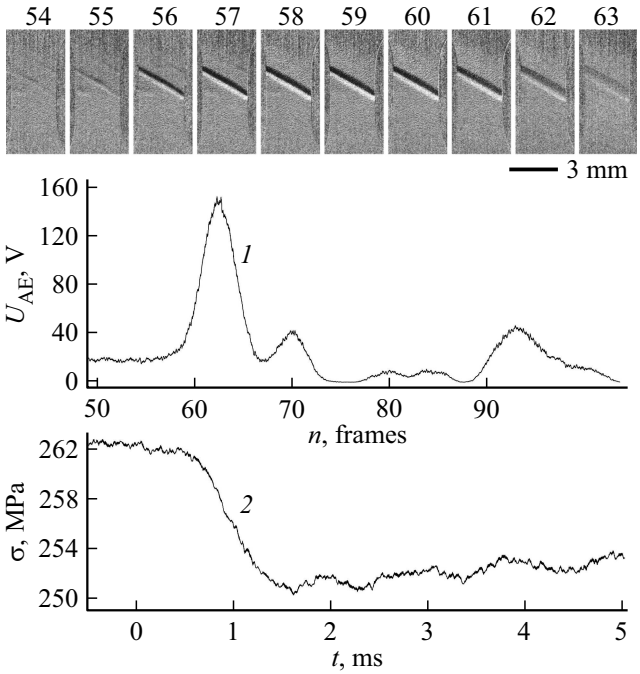

Figure 4. Acoustic (*1*) and force (*2*) responses to the formation of a deformation band. The top insert shows corresponding fragment of the video record at a rate of 2000 fps, n is number of the video record frame.

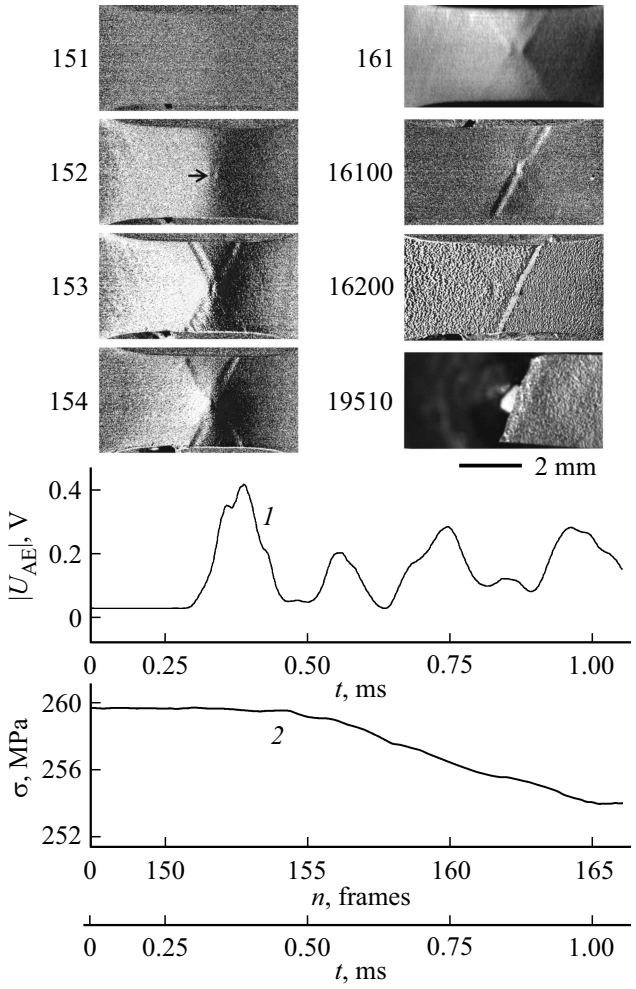

Figure 5. $|U_{AE}(t)|$ (Time dependencies of the AE signal modulus *1*) and the unloading jump σ (*2*) under an indenter shock in the process of uniaxial tension of the AMg6-I alloy sample. The insert shows a fragment of video record of formation of crossing associated bands from the moment of shock till sample destruction along one of the bands. The arrow shows a mark formed by the coming out of the band tip to the sample side opposite to the indenter. Frames 151-154, 16 100, 16 200 are obtained using computer processing of images, other frames are not computer-processed.

manifested in the threshold and multiple character of these responses, which are fading not exponentially (as in linear systems) but in the form of successive stress jumps and bursts of AE signal similar to residual shocks (aftershocks) after the main earthquake [13,14].

To study dynamics of the primary band initiated by a shock impact and its correlation with subsequent bands involved in the development of macroscopic deformation jump on the loading curve, the rate of video recording was increased to 20 000 fps. It follows from the results of video recording that on the surface opposite to the indenter in the center of working part of the sample first a mark appears (shown with arrow in Fig. 5), from which then two associated deformation bands „grow" at angles of $\pm 30^\circ$ in relation to the normal cross-section, and a local region of their crossing is located opposite to the indent. Then a stress decrease in the force response starts (see Fig. 5, curve *2*), which is consistent with conclusions of [9,15]. It can be seen from the shape of AE signal that maximum of the signal corresponds to the moment of the mark emergence (frame 152) and start of the AE signal corresponds to the previous frame (frame 151) that has no mark yet. According to [9], amplitude of the AE signal corresponds to the moment of embryo band coming out at the opposite surface. It follows from the results of high-speed video and measurement of the AE signal, that the x-shaped mark is resulted from the coming out of tips of the associated deformation bands generated by the indenter shock at the surface opposite to the indenter, and the start of shock is considered at the start of AE signal, which gives the upper estimated time of band propagation of $\Delta t = 50\,\mu$s and the lower estimated velocity of its tip of $v_t \approx w/\Delta t \approx 10$ m/s, where $w = 0.5$ mm is thickness of the sample.

It is worth to note that experimental studies of the deformation band geometry in alloys that demonstrate discontinuous deformation allowed identifying deformation bands of two types in flat samples: bands oriented at an angle of 90° on the front surface and an angle of $\beta = 55-63^\circ$ to the axis of tension on the side surface (bands of type I) and bands oriented at an angle of β to the axis of tension on the front surface and an angle of 90° on the side surface (bands of type II) [15] (for an isotropic plastically deformable material $\beta = \text{arctg}\sqrt{2} = 54^\circ 44'$ [16]). In samples with a ratio of $d/w > 5$ bands of type II prevail ($d = 3$ mm is sample thickness). The main (shear) crack always develops along one of the associated deformation bands generated by the indenter shock (Fig. 5).

The formation of associated deformation bands initiated by shock indentation is observed at the intermittent section of the tensile curve in the last third of any plateau starting from the 2–3-rd plateau, i.e. above the $\sigma \approx 210-350$ MPa $\approx (1.3-1.4)\sigma_{02}$, where $\sigma_{02} \approx 160$ MPa is offset yield strength of the AMg6 alloy. It means that for the nucleation and propagation of bands, it is necessary to overcome a certain critical level of internal stress in the material, which increases on the plateau after a successive jump causing their fast relaxation.

Work-hardened samples of AMg-II, that do not demonstrate the PLC discontinuous deformation, also demonstrate no induced jumps after the indenter shock in the process of loading. The indenter shock in the process of uniaxial tension at a stress of 250–350 MPa produces on the opposite side of the sample a surface deformation relief of „orange peel" type in an approximately sixty-degree sector that reflects the distribution of tangential stresses.

4. Discussion of results

Based on the obtained results, the following scheme can be suggested for the formation of bands initiated by

the indenter shock. With a shock impact on the sample surface deformed by a uniaxial tension, the indenter tip, as a concentrator of stress, generates two associated bands of type II (Fig. 6). Before the coming out onto the surface opposite to the indenter, boundaries of the bands inside the material body have a parabolic shape. When a tip of one of these bands come out on the opposite surface monitored by video camera, first a mark appears in the form of a line section, then the coming out of the associated band tip makes the mark x-shaped (see insert in Fig. 6). With this scheme of band formation the mark is located exactly opposite the indenter tip, which is consistent with the data of observations. As a results of competition between the associated bands one of them will prevail and become a trigger of the development of macroscopic deformation jump on the loading curve due to the generated secondary bands by the cascade mechanism described in [17].

The obtained results are indicative of the involvement of macrolocalized deformation bands in the structure of the plastic zone under the indenter in the conditions of contact shock. In the case of static indentation of an isotropic material the plastic zone of a roundish shape (close to the semi-ellipsoid shape) with a size comparable to the indent size (0.1–0.2 mm) is suspected to be located behind the zone of hydrostatic compression, which is immediately under the indenter tip. If an alloy demonstrating the PLC effect is shock-indented, the local area under the indenter generates two deformation bands in associated directions of maximum tangential stresses, which cross the entire cross-section of the sample. Their sources are in the region of peak of the tangential stresses approximately at a distance of about the depth of indent under the indenter.

The analysis of self-consistent shifts in the crossing associated bands in accordance with the crosswise scheme, that has been performed in [18,19] in the context of studying the mechanism of plastic deformation in the neck, has shown that in the region of band crossing a local zone of omnidirectional tension is formed and conditions are created for the nucleation of crack as an initial phase of the destruction. Such a mechanism makes it possible to explain the formation of a local valley (mesoscopic neck) in the center of band crossing (see the arrow in the insert in Fig. 6, bottom right) and subsequent development of the main shear crack along one of the associated band (see Fig. 5). Thus, the shock indentation creates not only an indent on the alloy surface and a plastic zone with a size comparable with the indent depth but also bands of macrolocalized deformation with a length of several millimeters propagating into the material body, which evolution causes nucleation and development of the main shear crack.

It is worth to note that according to the data of electron-microscopic studies [20,21] the dislocation structure of Al–Mg plastic deformable alloys with a magnesium percentage of 3–6%, in contrast to the pure aluminum, is characterized by almost uniform distribution of dislocation tangles, and with growing content of Mg the frequency of dislocation intersections increases, which, in turn, increases

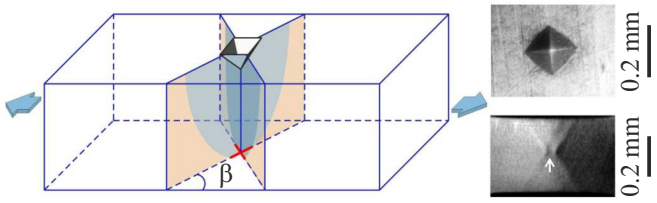

Figure 6. Scheme of formation of associated embryo bands under the indenter. β (54°44′ [16]) is angle between the plane of maximum tangential stresses and the axis of tension. The insert on the right shows the indent after the shock (top) and the x-shaped structure of the associated deformation bands on the opposite surface of a flat sample (bottom). The arrow shows the valley in the region of bands crossing.

the bulk concentration of uniformly distributed Frank–Read sources (f–P) and results in a growth of density of mobile dislocations [22]. On one hand, this creates a strengthening effect, and on the other hand, under certain conditions, it increases the probability of formation of a spatial structure, the nucleation wave.

According to the most general model of morphogenesis [23], the formation of spatial structure in an active distributed system is possible provided that the action range of the activator l used for the positive feedback is considerably less than the size of the inhibitor L used for the negative feedback; then an avalanche-like increase of the activator takes place with a typical size of $d_a \approx 2\pi(lL)^{1/2}$ that characterizes the scale of the spatially-inhomogeneous state [24]. l in a strained crystal is determined by the size of dislocation source and L is determined by the scale of structure of dislocation brake forces.

In the process of development of a macroscopically localized avalanche of dislocations that contains the excess of dislocations of one mechanical sign („mechanical charge"), in the conditions of uniaxial tension a bending moment increases in the sample [25,26], which impedes the propagation of the dislocation avalanche (negative feedback). The bending moment is relaxed due to the spontaneous formation of the opposite mechanical charge. In this situation, long-range fields of stress related to misalignment of the deformation created by the propagating band act as an inhibitor.

With an assumption that the inhibitor size is equal to the size of sample, $L \approx 6$ mm, and the typical scale of the dissipative structure is equal to the bandwidth at the early phase of development, $d_a \approx 0.3$ mm, the estimated size of activator, the active dislocation source, is $l = d^2/(4\pi^2 L) \approx 0.4\,\mu$m. According to [27], length of the pile-up of dislocations in the plane of gliding is determined by the following relationship

$$l_0 = \frac{NGb}{\pi\sigma k}, \tag{2}$$

where N is number of dislocations, G is shear modulus, b is Burgers vector, $k = 1$ for edge dislocations and

$k = 1-\nu$ for screw dislocations and ν is Poisson ratio. By assuming the stress σ exceeding the activation stress of the dislocation source of F–R type, that generates a pile-up of $N \approx 20$ [27] and substituting to (2) $G = 28$ GPa, $b = 0.286$ nm, $\nu = 0.33$, we get $l_0 \approx 0.36\,\mu$m for a pile-up of screw dislocations and $l_0 \approx 0.23\,\mu$m for a pile-up of edge dislocations, which is better than an order of magnitude consistent with the estimate of the activator size ($l \approx 0.4\,\mu$m). It worth to note that according to [28], base of the F–R source is $L_{\mathrm{FR}} \approx 10^3 b/8$ and the critical stress of source activation is $\sigma^* \approx Gb/L_{\mathrm{FR}} \approx 224$ MPa, i. e. it corresponds to the stress of first deformation bands nucleation and, respectively, the emergence of first jumps on the tensile curves of AMg6 alloy samples. The key role of multiplication of dislocations in the formation of deformation bands is established in [29], therefore it can be assumed that the mechanism of formation and propagation of deformation bands is related to collective activation of F–R dislocation sources.

As noted above, work-hardened samples (AMg-II) demonstrate no PLC effect and induced jumps of deformation after the indenter shock. High initial density of dislocations ($\sim 10^{12}\,\mathrm{cm}^{-2}$) and, respectively, submicroscopic average distance between dislocations ($\sim 10\,\mathrm{nm} \ll l$) suppresses the processes of dislocation nucleation and, as a consequence, formation of macrolocalized deformation bands. Plastic deformation in such „constrained“ conditions takes place due to the separation of dislocations from stops (impurity atoms and forest dislocations), precipitate cutting and climb, taking into account high concentration of deformation vacancies and second-phase precipitation after severe plastic deformation in alloys of the Al–Mg system [30,31]. Thus, due to high density of dislocations no deformation bans are formed in the work-hardened AMg6-II alloy. Inhomogeneity of plastic deformation manifests at the level of individual grains du to the intragranular gliding in accordance with the above-listed mechanisms, which explains qualitatively the deformation relief in the form of „orange peel“ and the absence of development of plastic instabilities at the macrolevel, i.e. PLC deformation bands.

Let us estimate the order of magnitude of main parameters of the shock indentation: the deformation rate, the loading rate and the time of contact interaction. In the case of elastic collision of the indenter with the flat sample it is considered that the ratio between the contact force P and the approach h remains the same as in the static case. When indenting by prismatic or conical indenters, this dependence is quadratic [32],

$$P(t) = kh^2(t), \tag{3}$$

where k is a parameter that depends on elastic properties of the material and the indenter geometry, and time dependence of the approach $h(t)$ is a solution to the dynamics equation

$$m\ddot{h} = -kh^2. \tag{4}$$

After the first integration of equation (4) the velocity of indenter penetration can be determined as follows

$$v(t) = \sqrt{v_0^2 - \frac{2kh^3(t)}{3m}}. \tag{5}$$

The approach h achieves it maximum h_0 at the moment of time $t = \tau_0$, when the approach velocity is zero. Hence,

$$h_0 = \left(\frac{3mv_0^2}{2k}\right)^{1/3} = \left(\frac{3W}{k}\right)^{1/3}, \tag{6}$$

where $W = mv_0^2/2$ is kinetic energy of the indenter before the contact shock. To calculate the duration of indenter shock penetration τ_0, equation (5) is to be integrated from the moment of shock start to the moment of maximum approach

$$\tau_0 = \int_0^{h_0} \frac{dh}{\sqrt{v_0^2 - \frac{2kh^3}{3m}}}. \tag{7}$$

It is convenient to introduce a dimensionless variable $x = h/h_0$ for the integration. Then

$$\tau_0 = \frac{h_0}{v_0} \int_0^1 \frac{dx}{\sqrt{1-x^3}}, \tag{8}$$

and by calculating the integral via gamma-function, we get

$$\tau_0 = \frac{h_0\sqrt{\pi}\,\Gamma\left(\frac{4}{3}\right)}{v_0\Gamma\left(\frac{5}{6}\right)} \approx 1.40218\,\frac{h_0}{v_0}. \tag{9}$$

By excluding the constant k from formulae (3) and (5), the ratio is derived between the kinetic energy of the indenter and the maximum shock force

$$P_{\max} = kh_0^2 = 3W/h_0. \tag{10}$$

Below is the comparison between the derived formulae and the data presented in literature. In [33] on the basis of theoretical and experimental studies of elastic-plastic shock of a rigid indenter with an apex angle from 50 to 150° to a deformable half-space estimates are obtained for the time of shock τ_0 and the maximum force of shock $P_{\max}$

$$\tau_0 = 1.42h_{\mathrm{pl}}/v_0, \tag{11}$$

$$P_{\max} \approx 1.34mv_0^2/h_{\mathrm{pl}} = 2.68W/h_{\mathrm{pl}}, \tag{12}$$

which are well consistent with the derived formulae (9) and (10) if the maximum approach is taken equal to the depth of plastic indent h_{pl}, i. e. $h_0 \approx h_{\mathrm{pl}}$.

To obtain quantitative estimates, assume that according to the results of lateral recording the initial velocity of indenter is $v_0 \approx 1$ m/s, therefore $W = mv_0^2/2 = 2 \cdot 10^{-3}$ J, where $m = 4$ g is weight of the indenter; time of approach is $\tau_0 \approx 50\,\mu$s according to video recording results and measurements of AE signal and the typical indent diagonal

after the shock contact is $d \approx 200\,\mu$m. Taking into account that the indent depth is related to its diagonal as $h_{\text{pl}} = d/\left(2\sqrt{2}\,\text{tg}(\alpha/2)\right) \approx d/7 \approx 30\,\mu$m, where $\alpha = 136°$, from formulae (11) and (12) the estimate of the shock approach time is $\tau_0 \approx 42\,\mu$s, which is well consistent with the experiment ($\sim 50\,\mu$s), and the estimate of maximum shock force is $P_{\max} \approx 180$ N.

The obtained data of *in situ* investigations of dynamics and geometry of deformation bands in the process of shock indentation was compared with results of computer modeling of the distribution of stress and deformations field at a shock interaction of the indenter with the surface of aluminum alloy deformed by uniaxial tension over the offset yield strength. It was assumed that the stress distribution corresponds to the static case because the lag time $\delta t = w/c \approx 0.2\,\mu$s is considerably less than the approach time $\delta t \ll \tau_0$ (here $c \approx 3$ km/s is sound velocity). Modeling was carried out in the COMSOL Multiphysics software package using the Solid mechanics module and the Contact Pairs method. This model based on the von Mises' yield criterion [34] assumed that at a tensile stress of $\sigma = 250$ MPa the front surface of sample (3×6 mm) was subjected to an impact of a quadrilateral pyramid with an apex angle of 136° with a linearly increasing force for $50\,\mu$s up to the maximum of $P_{\max} = 180$ N. The functional relation between deformation and stress was defined by means of the digitized loading curve $\varepsilon(\sigma)$ in Fig. 1.

Fig. 7, *a* shows distribution of the plastic deformation field $\Delta\delta(x, y)$ on the surface of the sample opposite to indenter at the moment of maximum approach, where $\Delta\delta(x, y) = \delta(x, y) - \delta_0$ is increment of the relative deformation caused by the indenter shock, $\delta(x, y)$ is deformation field on the opposite surface of the sample, δ_0 is uniform field of deformation at a stress of $\sigma = 250$ MPa before the indenter shock. It can be seen that the most intensive deformation takes place in directions of maximum tangential stresses associated to each other in a crosswise scheme, which have angles to the tension axis of 54°44′ and 125°46′ [16], respectively, which is well consistent with the geometry of associated deformation bands in the AMg6-I alloy (Fig. 7, *b*) and with the sixty-degree sector covered by the „orange peel" in the AMg6-II alloy (Fig. 7, *c*) that demonstrates no PLC effect.

Now let us estimate values of dynamic hardness $H_{\text{Vd}} = 1.854 P_{\max}/d^2$, loading rate $\dot{\sigma}_{\text{imp}} = P_{\max}/(S\tau_0)$, where $S = \frac{1}{2}\,d^2/\sin(\alpha/2)$ is conditional area of the lateral surface of the indent and average deformation rate $\dot{\varepsilon}_{\text{imp}} = \langle h^{-1} dh/dt \rangle \approx v_0/h_0$. Taking into account the values of $v_0 \approx 1$ ms, $\tau_0 \approx 42\,\mu$s, $P_{\max} = 180$ N, $d \approx 200\,\mu$m, $h_0 \approx 30\,\mu$m obtained above, the obtained estimate of the maximum dynamic hardness is $H_{\text{Vd}} \approx 8.4$ GPa, which is an order of magnitude higher than the static hardness of the AMg6-I alloy of $H_{\text{Vst}} \approx 800$ MPa, the estimate of maximum loading rate is $\dot{\sigma}_{\text{imp}} \approx 2 \cdot 10^5$ GPa/s and the estimate of average deformation rate is $\dot{\varepsilon}_{\text{imp}} \approx 3 \cdot 10^4\,\text{s}^{-1}$.

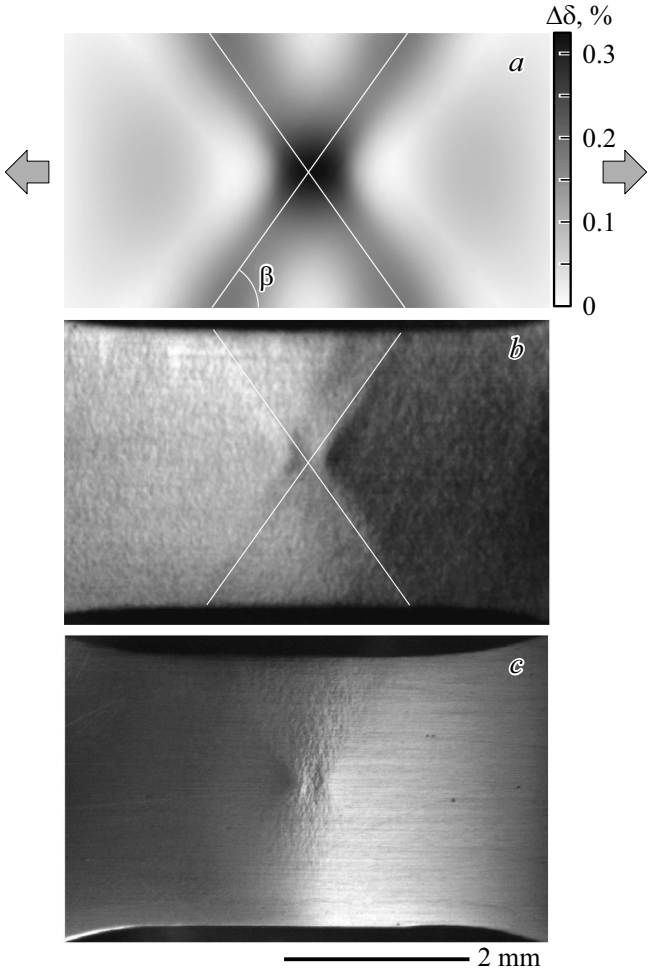

Figure 7. Deformation field on the surface opposite to the shock in conditions of uniaxial tension over the offset yield strength: *a*) obtained by computer modeling; *b* and *c*) obtained experimentally in AMg6-I and AMg6-II alloys, respectively. Directions of maximum tangential stresses associated in a crosswise scheme are shown in figures *a* and *b*. $\beta = \text{arctg}\,\sqrt{2} = 54°44'$ [16].

In respect to this region of deformation and loading rates in [35] a model of incubation time is suggested on the basis of the „dislocation starvation" concept in the conditions of high-rate uniaxial deformation (see also [36]) and erosion destruction [37], which can be also applied to the case under consideration, which is an example of high-rate local deformation with dynamic characteristic considerably higher than those of the static case.

It is worth to note that minimum flux density of the energy transferred to the material by the shock indentation is $F = W/(A\tau_0) \approx (2-3) \cdot 10^5$ W/cm^2, where $A = d^2/2$ is projected area of the final indent, which is comparable with the laser emission flux density of a pulse laser „injection" of the AMg6 alloy surface causing formation of deformation bands [11]. In the case of erosion wear of the surface the energy of indenter shock is comparable with the energy of a high-velocity particle with a velocity of 250 m/s (900 km/h), a density of ~ 3 g/cm^2 and a size of about 0.3 mm, which is

typical, for example, for volcanic ash [38] in the condition of interaction with the skin of aircraft.

5. Conclusion

Deformation and acoustic responses were investigated experimentally for shock indentation of AMg6 polycrystalline aluminum-magnesium alloy deformed by uniaxial tension over the offset yield strength. Samples in two structural states were studied: recrystallized (AMg6-I) with an initial dislocation density of $\sim 10^8\,\mathrm{cm}^{-2}$ and work-hardened (AMg6-II) with a dislocation density of $\sim 10^{12}\,\mathrm{cm}^{-2}$. In the absence of shock impact the AMg6-I samples demonstrated Portevin–Le Chatelier discontinuous deformation and AMg6-II samples deformed without jumps and deformation bands, except for the phase of predestruction.

Main results can be divided into two groups related to dynamic and nonlinear responses for the shock indentation. The first group includes the following:

– peak dynamic hardness more than an order of magnitude higher than the static hardness for the AMg6-I alloy and almost 7 times higher than the static hardness for the AMg6-II, peak rates of stress growth of $\sim 2 \cdot 10^5\,\mathrm{GPa/s}$ and rates of local deformation of $\sim 3 \cdot 10^4\,\mathrm{s}^{-1}$ make the shock indentation to be classified as a dynamic effect of macroplastic deformation of the „dynamic yield tooth“ type and other inertial factors of defect dynamics;

– in the AMg6-I alloy, in addition to the plastic indent, the shock indentation of the sample deformed in the conditions of uniaxial tension results in a deformation macrojump on the loading curve due to formation and propagation of PLC deformation bands. In the first tens of microseconds two bands of macrolocalized deformation are generated under the indenter and propagated through the cross section of the sample in associated directions of maximum tangential stresses. Then, after a contact shock, boundaries of these bands generate secondary bands, which cause development of the deformation jump with an amplitude of several percents. As it is found, the main crack always propagates along one of the associated bands generated under the indenter.

The AMg6-I alloy, in addition to the PLC effect, demonstrates nonlinear deformation and acoustic responses to the shock impact that form the second group of phenomena:

– the deformation response has a threshold and multiple character: amplitude of the deformation jump induced by the shock has a strongly nonlinear dependence on the moment of shock in relation to the start of the plateau on the stepwise loading curve. The multiple character is manifested in the fact that a single indenter shock with a duration of $\sim 50-100\,\mu\mathrm{s}$ is a trigger for nucleation and propagation of about ten or more PLC deformation bands within about $\sim 1\,\mathrm{s}$ after the shock, i. e. $\sim 10^4$ times greater duration of the shock impact;

– the force and acoustic responses are fading not exponentially as in linear systems but demonstrating a more complicated behavior in the form successive stress drops synchronized with bursts of the AE signal, which correspond to the formation of deformation bands.

In the AMg6-II alloy that demonstrates no PLC effect the shock indentation does not cause formation of deformation bands and jumps on the deformation curve. Thus, in this study it is shown that bands of macrolocalized deformation are a latent bulk type of erosion damage, which decreases durability of the alloy that demonstrates the PLC effect and can cause its sudden destruction.

Funding

This study was supported by the Russian Science Foundation (project No. 22-22-00692) using the equipment of the Center of Equipment Sharing of the Derzhavin State University of Tambov.

Conflict of interest

The authors declare that they have no conflict of interest.

References

[1] L.P. Kubin, C. Fressengeas, G. Ananthakrishna. Dislocat. Solids **11**, 101 (2002).
[2] E. Rizzi, P. Hahner. Int. J. Plast. **20**, *1*, 121 (2004).
[3] A.J. Yilmaz. Sci. Technol. Adv. Mater. **12**, *6*, 063001 (2011).
[4] A.W. McReynolds. Metals Transact. **1**, 32 (1949).
[5] K. Chihab, Y. Estrin, L.P. Kubin, J. Vergnol. Scripta Metallurg. **21**, *2*, 203 (1987).
[6] W. Tong, H. Tao, N. Zhang, L.G. Hector. Scripta Mater. **53**, *1*, 87 (2005).
[7] G.F. Xiang, Q.C. Zhang, H.W. Liu, X.P. Wu, X.Y. Ju. Scripta Mater. **56**, *8*, 721 (2007).
[8] M.M. Krishtal, A.K. Khrustalev, A.V. Volkov, S.A. Borodin, Dokl. RAN **426**, *1*, 36 (2009). (in Russian).
[9] A.A. Shibkov, M.A. Lebyodkin, T.A. Lebedkina, M.F. Gasanov, A.E. Zolotov, A.A. Denisov. Phys. Rev. E **102**, *4*, 043003 (2020).
[10] A.A. Shibkov, A.A. Mazilkin, S.G. Protasova, D.V. Mikhlik, A.E. Zolotov, M.A. Zheltov, A.V. Shuklinov, Deformatsiya i razrusheniya materialov, *6*, 12 (2008). (in Russian).
[11] A.A. Shibkov, A.E. Zolotov, M.F. Gasanov, M.A. Zheltov, K.A. Proskuryakov. Phys. Solid State **60**, *9*, 1674 (2018).
[12] A.A. Shibkov, A.A. Denisov, A.E. Zolotov, S.S. Kochegarov. Phys. Solid State **59**, *1*, 98 (2018).
[13] J. Weiss, J.-R. Grasso, M.-C. Miguel, A. Vespignani, S. Zapperi. Mater. Sci. Eng. A **309–310**, 360 (2001).
[14] J. Weiss, F. Louchet. Scripta Mater. **54**, *5*, 747 (2006).
[15] A.A. Shibkov, M.A. Zheltov, M.F. Gasanov, A.E. Zolotov, A.A. Denisov, M.A. Lebyodkin. Mater. Sci. Eng. A **772**, 138777 (2020).
[16] R. Hill. The Mathematical Theory of Plasticity. Clarendon Press, Oxford (1950).
[17] A.A. Shibkov, M.F. Gasanov, M.A. Zheltov, A.E. Zolotov, V.I. Ivolgin. Int. J. Plast. **86**, 37 (2016).

[18] V.E. Panin, L.S. Derevyagina, E.E. Deryugin, A.V. Panin, S.V. Panin, N.A. Antipina. Phiz. mezomekh **6**, *6*, 97 (2003). (in Russian).
[19] L.S. Derevyagina, V.E. Panin, A.I. Gordienko. Phiz. mezomekh **10**, *4*, 59 (2007). (in Russian).
[20] D.A. Hughes. Acta Metallurg. Mater. **41**, *5*, 1421 (1993).
[21] J. Gubicza, N.Q. Chinh, Z. Horita, T.G. Langdon. Mater. Sci. Eng. A **387**–**389**, 55 (2004).
[22] G. Horváth, N.Q. Chinh, J. Gubicza, J. Lendvai. Mater. Sci. Eng. A **445**–**446**, 186 (2007).
[23] A.M. Turing. Phil. Trans. Roy. Soc. London. A **237**, *641*, 37 (1952).
[24] B.S. Kerner, V.V. Osipov. Phys.-Usp. **33**, *9*, 679 (1990).
[25] H. Neuhäuser. Dislocation in Solids / Ed. F.R.N. Nabarro. North Holland Company **6**, 319 (1983).
[26] P. Hähner, A. Ziegenbein, E. Rizzi, H. Neuhäuser. Phys. Rev. B **65**, *13*, 134109 (2002).
[27] R.W.K. Honeycombe. Plastic Deformation of Metals. Nature (1932).
[28] J.P. Hirth, J. Lothe. Theory of Dislocations. Cambridge University Press (1968).
[29] A.A. Shibkov, A.E. Zolotov. JETP Lett. **90**, *5*, 370 (2009).
[30] M.Yu. Murashkin, A.R. Kil'mametov, R.Z. Valiev. Phys. Met. Metallography **106**, *1*, 90 (2008).
[31] M.V. Markushev, M.Yu. Murashkin. Phys. Met. Metallography **98**, *2*, 221 (2004).
[32] Yu.V. Kolesnikov, E.M. Morozov. Mekhanika kontaktnogo razrusheniya, LKI, M., (2012), 224 p. (in Russian).
[33] G.S. Batuev, Yu.V. Golubkov, A.K. Efremov, N.I. Malinin, Inzhenernye metody issledovaniya udarnykh protsessov, Mashinostroenie, M., (1977), 240 p. (in Russian).
[34] B. Paul. Macroscopic Criteria for Plastic Flow and Brittle Fracture. In: Fracture — A Treatise. V. 2. / Ed. H. Liebowitz. Academic Press, London (1968).
[35] N. Selyutina, E.N. Borodin, Y. Petrov, A.E. Mayer. Int. J. Plast. **82**, 97 (2016).
[36] N.S. Selyutina, Yu.V. Petrov. Phys. Solid State **60**, *2*, 244 (2018).
[37] A.D. Evstifeev, Yu.V. Petrov, N.A. Kazarinov, R.R. Valiev. Phys. Solid State **60**, *12*, 2363 (2018).
[38] F. Prata, B. Rose. Volcanic Ash Hazards to Aviation. In: The encyclopedia of volcanoes. / Ed. H. Sigurdsson. 2nd ed. Academic Press (2015). Ch. 52. P. 911.

Translated by Y.Alekseev